Available online at www.sciencedirect.com
SCIENCE DIRECT®
Fluid Phase Equilibria 221 (2004) 175–187
FLUID PHASE EQUILIBRIA
www.elsevier.com/locate/fluid

# Equilibrium hydrate formation conditions for hydrotrope–water–natural gas systems

Nimalan Gnanendran*, Robert Amin

*Woodside Research Foundation, Department of Petroleum Engineering, Curtin University of Technology, GPO Box U1987, Perth, WA 6845, Australia*

Received 4 July 2003; received in revised form 5 April 2004; accepted 5 April 2004

Available online 1 July 2004

**Abstract**

The thermodynamic influence of hydrotrope *para*-toluene sulfonic acid (*p*TSA), when present in water–natural gas–hydrate system, is reported here for the first time. Hydrotropes are aromatic compounds amphiphilic in nature, yet differ from classical surfactants with their small hydrophobic part and comparatively larger hydrophilic part. The presence of surfactants in hydrate systems were reported not to influence the equilibrium thermodynamics of hydrate formation, i.e., the presence of surfactants did not shift the pure water–gas–hydrate equilibrium curves. This work finds *p*TSA, a hydrotrope and a surface-active agent, to influence the hydrate forming thermodynamics. The water–gas–hydrate equilibrium curves for three different additive concentrations in water were obtained from isochoric 'temperature cycling' experiments in a state-of-the-art PVT cell. The hydrotrope aggregation behaviour in water was incorporated, for the first time, into the classical statistical thermodynamic hydrate equilibrium prediction model proposed by van der Waals and Platteeuw [Am. Inst. Chem. Eng. 32 (1986) 1321]. The micelle size, or aggregation number, of hydrotropes was taken as the only adjustable parameter in the model, which was adjusted according to the hydrate equilibrium experiment data to give a minimum average absolute deviation (AAD) fit between the model and the experiment values. A relationship was subsequently developed for the micelle size and *p*TSA concentration, making the scheme a priori prediction model for concentrations within the tested region.


*Keywords:* Model; Hydrates; Natural gas; Hydrotrope; Activity coefficient; Hydrate promoters; *p*-Toluenesulfonic acid; Micelle

## 1. Introduction

Gas hydrates are a variety of chemical compounds known as clathrates, where small gas molecules are stabilised in hydrogen-bonded water molecule cages of sizes less than 9 Å. Gas hydrates resemble ice and exhibit similar physical properties as ice, but they are formed at much elevated temperatures than the ice point, at moderate to high pressures. A substantial amount of research on gas hydrates is related to the petroleum industry, as they are found to cause blockages in process pipelines and equipment. The aim of most of this research work related to gas hydrates is to understand the thermodynamics and kinetics involved in hydrate formation, and to establish suitable hydrate prevention methods to be used with different oil and gas systems. The thermodynamics of hydrate formation has been clearly established for pure water and most hydrocarbon gas and liquid systems at normal industrial operating pressure–temperature conditions. There has also been studies related to hydrate formation equilibrium prediction in hydrate inhibition systems such as aqueous electrolyte solutions [2] and anti-freeze systems [3,4]. The hydrate inhibitors, which alter the hydrate formation equilibrium by altering the water properties, are referred to as thermodynamic inhibitors; these inhibitors shift the equilibrium curve, thus forming hydrates at lower temperatures at a given pressure. Hydrate formation kinetics involves the study of nucleation and crystal growth, and still provides a great challenge to researchers. This is mainly due to the stochastic nature of hydrate formation, and the inherent difficulties involved in identifying and measuring all the parameters influencing hydrate nucleation and subsequent hydrate crystal growth. Several studies have

* Corresponding author. Tel.: +61-8-9266-3129; fax: +61-8-9266-4848.
*E-mail address:* nimalan@peteng.curtin.edu.au (N. Gnanendran).

0378-3812/$ – see front matter © 2004 Elsevier B.V. All rights reserved.
doi:10.1016/j.fluid.2004.04.013

made considerable progress in analysing the hydrate growth kinetics [5–7]. There are also studies related to kinetic inhibitors which prolong the nucleation time when added to a gas–water system [8,9]. Kinetic inhibitors have not yet been equally accepted as thermodynamic inhibitors in the industry, due to the uncertainties existing in predicting the hydrate formation kinetics. The recent work published on kinetic modelling of hydrate nucleation and growth based on crystallisation principles seems encouraging, as it incorporates the activity of additives such as hydrate inhibitors and hydrate promoters in hydrate systems [10–12].

There is also a growing research interest into the use of gas hydrates as a gas storage and transportation medium [13,14]. The research interest at Curtin University of Technology is also motivated towards this use. The key focus of using hydrates as a storage or/and transportation medium depends on the maximum possible gas storable in hydrates and the rate of formation of these hydrates. The maximum amount of gas storable in hydrates is limited by the theoretical gas to water ratio associated with the three hydrate structures. Hydrates structures I, II and H have an ideal gas to water molecular ratio of 8:46, 24:136 and 6:34, respectively [15]. Hydrates could be formed with gas components partially filling the cages, and also with un-reacted interstitial water remaining within the hydrates. Therefore the aim of any process utilising hydrates as a storage or/and transportation medium would be to achieve maximum possible water conversion to hydrates, closer to the ideal gas to water ratio, in the shortest possible time. Similar to hydrate inhibition, hydrate promotion has two distinct approaches, namely the thermodynamic hydrate promotion and the kinetic hydrate promotion. Thermodynamic hydrate promotion can be achieved by using hydrate promoters in the gas–water system to reduce the formation pressure at a given temperature, thus enabling hydrates to be formed at lower pressures. A typical example of such a chemical is 1,4-dioxane, which lowers the formation pressure at a given temperature when added to a methane–water system [16]. Another variation of this approach is to form structure H hydrates using structure H hydrate formers, which can theoretically store more gas [17]. Kinetic hydrate promotion is achieved by using additive chemicals, which reduces the hydrate nucleation time and increase the hydrate growth rate. Surface-active agents such as anionic surfactants [18] and hydrotropes [19] exhibit such properties. Researchers have suggested that such hydrate promoters could save energy costs of hydrate promotion schemes using stirring systems used for accelerating the usually sluggish hydrate formation process [20].

A typical natural gas forms structure II hydrates when subjected to hydrate formation conditions [21]. Therefore any process for storing and/or transporting natural gas by means of forming hydrates is limited to structure II hydrates, provided there is more than 1 mol% of propane and butane in the gas. The amount of gas to hydrate volume ratio theoretically achievable in structure II hydrates at standard conditions is found to be approximately 180:1. Therefore the challenge of using hydrates as a gas storage and/or transportation medium would be to achieve this gas to hydrate ratio at economic pressure–temperature conditions, at the highest possible formation rate. This could be achieved by selecting an appropriate hydrate-promoting chemical that would ideally lower the formation equilibrium pressure and increase the formation rate. The work in our laboratories is intended to achieve the above with the use of a hydrotrope additive in the water–gas–hydrate system. Hydrotropes are a class of compounds, though amphiphilic in character, have short hydrophobic regions and thus differ from classical surfactants, yet they display a substantial ability to solubilise non-polar compounds in water [22]. The hydrate promotion effect of the hydrotrope *para*-toluene sulfonic acid (*p*TSA), has been discussed in our previous publication, where gas to water ratio of the hydrates formed in the presence of *p*TSA in a natural gas–water system were measured [19].

The development of hydrate formation equilibrium curves, specifically the water–vapour–hydrate (Lw–V–H) lines, for a particular gas–water–additive system is vital for thermodynamic and subsequent kinetic modelling studies related to the hydrate promoter system. The thermodynamic influence of surfactants such as sodium lauryle sulfate on hydrate formation systems were suggested to be minimal, whereby hydrate formation equilibrium conditions remained the same as in a gas–water system [18,20,23,24]. However, the hydrotrope *p*TSA, when present in very small quantities in a water–natural gas–hydrate system, influenced the equilibrium hydrate formation conditions when subjected to an isochoric 'temperature cycling' experiment. An isochoric 'temperature cycling' experiment is a process of forming hydrates by decreasing the temperature in a gas–water system, while monitoring the pressure–temperature variation, and after formation dissociating the hydrates by increasing the temperature [15]. The experiments in Karaaslan et al. [23] indicate a similar characteristic of the anionic surfactant, linear alkyl benzene sulfonic acid (LABSA); however, the authors did not recognise the influence on hydrate dissociation thermodynamics as they had concentrated on the influence of different hydrate structures on the hydrate formation rate. Further, the exact formula of the LABSA was not reported in their publication, thus making it impossible for a definite comparison with *p*TSA.

In this work hydrate formation experiments were carried out in a state-of-the-art PVT cell with natural gas–*p*TSA/water systems. The temperature cycle curves were traversed to form and dissociate hydrates in quiescent *p*TSA–water–natural gas systems at different pressure levels to obtain hydrate equilibrium points. The equilibrium points obtained for three different *p*TSA concentrations showed a shift from the pure water–natural gas–hydrate equilibrium curve obtained from CSMHYD© [15]. The classical statistical thermodynamic approach proposed by van der Waals and Platteeuw [1] was used in our modelling. The UNIFAC group contribution method was used to determine the water activity in the presence of organic additive

*p*TSA. The effect of the self-aggregation phenomena of the surface-active *p*TSA molecules was incorporated in the model by correlating it to the chemical potential of water.

## 2. Model formulation

The modelling of the hydrate formation equilibrium prediction for the *p*TSA–water–natural gas system was attempted in two steps, initially a model for the pure water–natural gas system was developed and subsequently the model was extended to incorporate the features of *p*TSA in the liquid phase. The activity of *p*TSA in water and the aggregation phenomena of surface-active *p*TSA molecules were considered in developing the model.

The model for the prediction of equilibrium hydrate formation conditions in pure water–natural gas systems was based on the scheme proposed by van der Waals and Platteeuw [1]. This statistical thermodynamic scheme was based on the Langmuir gas adsorption analogy. The scheme was later refined by Parrish and Prausnitz [21] to be used with natural gas mixtures. Subsequently several researchers simplified the scheme with appropriate assumptions for the water phase chemical potential [25,26]. This pure water scheme has been modified to incorporate other chemicals in the water phase, and is widely used for predicting hydrate formation in the presence of inhibitors like methanol [3] and electrolytes [2] with suitable variations to the liquid phase activity. The model used in this work assumes that structure II hydrates are formed, as it is this type of structure which would form in the presence of natural gas components such as propane and iso-butane [21]. The model was developed to solve at a given temperature and gas composition to find the hydrate formation pressure using an iterative approach similar to the one proposed by Sloan [15].

### 2.1. Model for pure water–natural gas system

The classical statistical thermodynamic modelling of pure water–gas–hydrate systems for equilibrium hydrate predictions is summarised in this sub-section, together with the assumptions. The thermodynamic conditions for hydrate formation prediction is based on the following criteria: gas hydrates should be in equilibrium with a water-rich liquid or ice phase if and only if the chemical potential of water in the hydrate ($\mu_W^H$) is equal to the chemical potential of water ($\mu_W^L$) in the liquid or ice phase:

$$\mu_W^H = \mu_W^L \tag{1}$$

For convenience the chemical potential difference between a theoretical empty water lattice $\mu_W^\beta$ and a liquid or hydrate lattice is compared:

$$\Delta\mu_W^H = \Delta\mu_W^L = \mu_W^\beta - \mu_W^H = \mu_W^\beta - \mu_W^L \tag{2}$$

#### 2.1.1. Chemical potential of water in the hydrate phase

Van der Waals and Platteeuw derived an expression for the chemical potential difference between a theoretical empty water lattice and a hydrate lattice, from the grand canonical partition function, which was based on the following assumptions:

- a cavity can only hold one guest molecule;
- the motion of a guest molecule in its cage is independent of the number and type of guest molecules present;
- interaction between host and guest molecules are weak van der Waals forces and extend only to the first shell of water molecules around each guest molecule (with the neglect also of guest–guest interactions between different cages);
- the hydrate lattice is not distorted by the guest molecule.

The fractional occupancy of hydrate forming component '*i*' in a hydrate cavity '*n*' is given by the following relationship (note: there are two types of cavities for sII hydrates):

$$\theta_{i,n} = \frac{C_{i,n} f_i}{1 + \sum_{j=1}^{m} C_{j,n} f_j} \tag{3}$$

The Langmuir constant accounts for the gas–water interaction in the cavity. Using the Lennard–Jones–Devonshire cell theory, van der Waals and Platteeuw [1] derived the Langmuir constant as

$$C_{k,n} = \frac{4\pi}{kT} \int_0^{R-a} \exp\left(\frac{-\omega(r)}{kT}\right) r^2 \, \mathrm{d}r \tag{4}$$

McKoy and Sinanoglu [27] derived the formula for cell potential $\omega(r)$ as

$$\omega(r) = 2z\varepsilon \left( \frac{\sigma^{12}}{R^{11} r} \left( \delta^{10} + \frac{a}{R} \delta^{11} \right) - \frac{\sigma^6}{R^5 r} \left( \delta^4 + \frac{a}{R} \delta^5 \right) \right) \tag{5}$$

where

$$\delta^N = \frac{1}{N} \left[ \left(1 - \frac{r}{R} - \frac{a}{R}\right)^{-N} - \left(1 + \frac{r}{R} - \frac{a}{R}\right)^{-N} \right] \tag{6}$$

Using the above correlations the chemical potential difference of water in hydrates and a theoretical empty hydrate lattice, $\Delta\mu_W^H$, is given by

$$\Delta\mu_W^H = \mu_W^\beta - \mu_W^H = RT \sum_n \nu_n \ln \left(1 - \sum_{i=1}^{p} \theta_{i_n}\right) \tag{7}$$

#### 2.1.2. Gas phase components

The fugacity of the hydrate forming components in the gas phase, $f_i$, was determined using the Soave–Redlich–Kwong (SRK) cubic equation-of-state [28], which is expressed in its *z* form as

$$z^3 - z^2 + (A - B - B^2)z - AB = 0 \tag{8}$$

where

$$A = \frac{aP}{(RT)^2} \quad \text{and} \quad B = \frac{bP}{RT} \tag{8.1}$$

For pure components constants '$a$' and '$b$' are given as follows:

$$a = \frac{0.42747 R^2 T_c^2}{P_c}\alpha(T) \tag{8.2}$$

$$\alpha(T) = \left(1 + \zeta\left(1 - \left(\frac{T}{T_c}\right)^{0.5}\right)\right)^2 \tag{8.3}$$

$$\zeta = 0.48508 + 1.55171\omega - 0.15613\omega^2 \tag{8.4}$$

$$b = \frac{0.08664 R T_c}{P_c} \tag{8.5}$$

For the natural gas mixture the above constants '$a$' and '$b$' were calculated using the two parameter mixing rules where binary interaction coefficients were obtained from Knapp and Doring [29]. The constants '$am$' and '$bm$' for the gas mixture are given by

$$am = \sum_i \sum_j y_i y_j a_i a_j (1 - \delta_{ij}) \tag{8.6}$$

$$bm = \sum_i y_i b_i \tag{8.7}$$

The fugacity of a component, $f_i$, in a phase mixture is defined as

$$f_i = y_i \phi_i P \tag{9}$$

The fugacity coefficients for the phase components can be found from the equation below, which was obtained from substituting the SRK equation of state in the basic fugacity coefficient equation:

$$\ln \phi_i = \frac{b_i}{bm}(z - 1) - \ln(z - B) - \frac{A}{B}\left(\frac{2\sum_j (a_i a_j)^{0.5}(1 - \delta_{i,j}) y_j}{am} - \frac{b_i}{bm}\right) \times \ln\left(1 + \frac{B}{z}\right) \tag{9.1}$$

*2.1.3. Chemical potential for the liquid water phase*

Holder et al. [25] proposed a simplified method to find the chemical potential difference of water in liquid or ice $\Delta\mu_W^L$, which is denoted as $\Delta\mu_W$ hereafter. Since chemical potential is a function of temperature and pressure only, the changes are given by

$$\mathrm{d}\left(\frac{\Delta\mu_W}{RT}\right) = -\left(\frac{\Delta\mu_W}{RT^2}\right)\mathrm{d}T + \left(\frac{\Delta v_W}{RT}\right)\mathrm{d}P \tag{10}$$

The integration yields

$$\left(\frac{\Delta\mu_W}{RT}\right) - \left(\frac{\Delta\mu_W}{RT}\right)_{T_0,P_0} = -\int_{T_0}^{T}\left(\frac{\Delta h_W}{RT^2}\right)\mathrm{d}T + \int_{P_0}^{P}\left(\frac{\Delta v_W}{RT}\right)\mathrm{d}P \tag{11}$$

$T_0$ and $P_0$ are the reference temperature and pressure, taken as 273.15 K and 1 atm, respectively. $\Delta v_W$ is taken as a constant, $\Delta v_W^0$, and the $\Delta h_W$ is related by the following equation given by [25]

$$\Delta h_W = \Delta h_W^0 + \int_{T_0}^{T} \Delta C_{P_W}^0 + q(T - T_0)\,\mathrm{d}T \tag{12}$$

*2.1.4. The activity of the water phase*

Eq. (11) applies for a pure condensed water phase, such as ice or liquid water without any solute. If the condensed water phase is not pure, the above equation should be modified to include a final term for the activity of water, $a_W$. The activity of water is expressed as

$$a_W = \gamma_W x_W \tag{13}$$

For very dilute solutions the activity coefficient of water, $\gamma_W$, can be taken as unity. The concentration of water, $x_W$, is also closer to unity, due to the low aqueous solubility of hydrate-forming hydrocarbons, but is not taken as unity in our case for the natural gas mixture. Instead the solubility of the components in the gas mixture is calculated using Henry's law. The solubility of a component '$i$' in the free water phase is given by the Henry's law equation:

$$x_i = \frac{f_i}{H_{i,W}\exp(P\bar{V}^\infty / R_c T)} \tag{14}$$

Fitted parameters of Henry's constants for most hydrate formers are given by the Krichevsky–Kasarnovsky correlation [30], where the universal gas constant $R_c$ has the units of cal $K^{-1}$ $Mol^{-1}$ and temperature is given in Kelvin. Recent researchers have also confirmed the validity of the Krichevsky–Kasarnovsky correlation [31]. The Krichevsky–Kasarnovsky correlation is expressed as

$$\ln H_{i,W} = \frac{H_{i,W}^{(0)}}{R_c} + \frac{H_{i,W}^{(1)}}{R_c T} + \frac{H_{i,W}^{(2)}}{R_c}\ln T + \frac{H_{i,W}^{(3)}}{R_c}T \tag{15}$$

In order to maintain the quantity $\Delta\mu_w$ as the difference between pure phases, the basic relation for chemical potential ($\mu_W = \mu_W^{\text{pure}} + RT\ln\gamma_W x_W$) is used to obtain an additional term on the right of Eq. (11) to obtain the following relationship for the chemical potential of the liquid water phase:

$$\left(\frac{\Delta\mu_W}{RT}\right) - \left(\frac{\Delta\mu_W}{RT}\right)_{T_0,P_0} = -\int_{T_0}^{T}\left(\frac{\Delta h_W}{RT^2}\right)\mathrm{d}T + \int_{P_0}^{P}\left(\frac{\Delta v_W}{RT}\right)\mathrm{d}P - \ln\gamma_W\left(1 - \sum_i x_i\right) \tag{16}$$

The above set of equations from (1) to (16) could be applied to a pure water–natural gas system to predict the hydrate formation pressure at a given temperature and natural gas composition.

### 2.2. Model for pTSA–water–natural gas system

The presence of *para*-toluene sulfonic acid in water changes the water activity. The effect of *p*TSA on the water activity is considered in two parts, initially *p*TSA is treated as an organic solute in water and the effect on water activity coefficient is determined, and then the effect of the self-aggregation phenomena of the hydrotrope, *p*TSA, is considered to determine the influence on the chemical potential of water.

#### 2.2.1. The activity of water in the presence of pTSA

The water activity coefficient in the presence of *p*TSA cannot be taken as unity as in the above for a pure water system. The UNIFAC group contribution-based method for liquid phase mixtures is used here for the prediction of activity coefficients of the components water and *p*TSA. The activity coefficient of component '*i*' is given by the combinatorial and residual terms as follows:

$$\ln \gamma_i = \ln \gamma_i^{\mathrm{C}} + \ln \gamma_i^{\mathrm{R}} \tag{17}$$

The combinatorial term is given by

$$\ln \gamma_i^{\mathrm{C}} = \ln \frac{\phi_i}{\chi_i} + 5q_i \ln \frac{\theta_i}{\phi_i} + \lambda_i - \frac{\phi_i}{\chi_i} \sum_j \chi_j \lambda_j \tag{18}$$

where

$$\lambda_i = 5(r_i - q_i) - r_i - 1 \tag{18.1}$$

$$\theta_i = \frac{q_i \chi_i}{\sum_j q_j \chi_j} \tag{18.2}$$

$$\phi_i = \frac{r_i \chi_i}{\sum_j r_j \chi_j} \tag{18.3}$$

Pure component area parameters $r_i$ and $q_i$ are, respectively, measures of molecular van der Waals volumes and molecular surface area [32,33]. Parameters $r_i$ and $q_i$ are calculated as the sum of the group volumes and group parameters $R_i$ and $Q_i$, as given below:

$$r_i = \sum_k V_k R_k \quad \text{and} \quad q_i = \sum_k V_k Q_k \tag{19}$$

where $V_k$, an integer, is the number of groups of type $k$ in molecule $i$.

The residual term of the activity coefficient is given by

$$\ln \gamma_i^{\mathrm{R}} = \sum_k V_k (\ln \Gamma_k - \ln \Gamma_k^i) \tag{20}$$

where $\Gamma_k^i$ is the residual activity coefficient of group '$k$' in a reference solution containing only molecules of type '$i$', which is given as

$$\ln \Gamma_k = q_i \left( 1 - \ln \left( \sum_j \theta_j \Psi_{ji} \right) - \sum_j \frac{\theta_j \Psi_{ij}}{\sum_k \theta_k \Psi_{kj}} \right) \tag{21}$$

and

$$\Psi_{ij} = \exp\left( \frac{-Ac_{ij}}{T} \right) \tag{21.1}$$

The component mole fraction, $\chi_i$, for the mixed phase and the pure phase are calculated separately along with the area fraction, $\theta_i$, to determine the residual activity coefficient. The activity of water $\gamma_{\mathrm{W}}$ in the presence of *p*TSA can be determined by solving Eqs. (17)–(21).

#### 2.2.2. The activity of water due to aggregation of pTSA

The self-aggregation phenomena (or the micellisation phenomena) relating to hydrotropes in a water–natural gas–hydrate system was discussed in our previous work [19]. The hydrate promoting qualities of hydrotropes as compared to surfactant solutions was emphasised based on an overall planar configuration of hydrophobic and hydrophilic regions exhibited by hydrotropes. Such an arrangement corresponds to an opened up micelle having greater accessibility to the hydrophobic regions than in spherical micelles for solubilising hydrocarbon components [22].

When water-soluble amphiphile molecules, or ions, are dissolved in water, the aggregation of amphiphiles occurs spontaneously and reversibly forming micelles [34]. According to Tanford, there is no universally accepted definition of micelle. Micelles can be small spheres or disks, oblate or polate ellipsoids, or long cylinders. They can also be in the form of bilayers, that is, two parallel layers of amphiphile molecules with the polar groups facing out. Micelle formation or micellisation is a fundamental property of surface-active agents where surface-active solutes form colloidal-sized clusters in solution.

The water activity equation can be written in the form given below when the micellisation of a surface active agent is taken into account [34]:

$$\mu_{\mathrm{W}} = \mu_{\mathrm{W}}^0 + RT \ln x_{\mathrm{W}} + RT \ln \gamma_{\mathrm{W}} - \frac{RT}{m} \ln \frac{x_0}{m} \tag{22}$$

The monomeric *p*TSA mole fraction in water is taken as $x_0$, and if the system is assumed to have an average size of '$m$' molecules per micelle or self-aggregation then $x_0/m$ is the micelle mole fraction of size, $m$, micelles in the liquid phase.

When the above micellisation behaviour, or self-aggregation behaviour, described in Eq. (22) is incorporated into the pure water chemical potential (Eq. (16)), it would take the following form:

$$\begin{aligned} &\left( \frac{\Delta \mu_{\mathrm{W}}}{RT} \right) - \left( \frac{\Delta \mu_{\mathrm{W}}}{RT} \right)_{T_0, P_0} \\ &\quad = -\int_{T_0}^{T} \left( \frac{\Delta h_{\mathrm{W}}}{RT^2} \right) \mathrm{d}T + \int_{P_0}^{P} \left( \frac{\Delta v_{\mathrm{W}}}{RT} \right) \mathrm{d}P \\ &\qquad -\ln \gamma_{\mathrm{W}} \left( 1 - x_0 - \sum_i x_i \right) \left( \frac{x_0}{m} \right)^{-(1/m)} \end{aligned} \tag{23}$$

Table 1
Mole fraction of natural gas components and critical properties

| Component | Mole fraction | Critical temperature (K) | Critical pressure (kPa) | Acentric factor, $\omega$ |
|---|---|---|---|---|
| $CO_2$ | 0.0219 | 304.1 | 7382 | 0.2276 |
| $N_2$ | 0.0260 | 126.1 | 3394 | 0.0403 |
| $CH_4$ | 0.8423 | 190.6 | 4599 | 0.0115 |
| $C_2H_6$ | 0.0679 | 305.4 | 4872 | 0.0995 |
| $C_3H_8$ | 0.0312 | 369.8 | 4248 | 0.1523 |
| $iC_4H_{10}$ | 0.0041 | 408.2 | 3648 | 0.1770 |
| $nC_4H_{10}$ | 0.0059 | 425.2 | 3796 | 0.2002 |
| $iC_5H_{12}$ | 0.0004 | 460.4 | 3058 | 0.2275 |
| $nC_5H_{12}$ | 0.0002 | 469.7 | 3370 | 0.2515 |
| $nC_6H_{14}$ | 0.0001 | 507.5 | 3025 | 0.3013 |

When calculating $x_0$, the effects of the gas components were neglected and when calculating $x_i$, the effects of dissolved *p*TSA in the water phase was neglected. The micelle size '*m*' is the only adjustable parameter in the model, which is adjusted according to the hydrate equilibrium experiment data to give a least square of errors fit between the model and the experiment values. Using the hydrate formation thermodynamic model equations from (1) to (15) and the water activity coefficient, $\gamma_W$, obtained from the UNIFAC group contribution method, along with Eq. (23), the hydrate formation equilibrium pressures at given temperatures can be predicted for various *p*TSA concentration solutions.

### 2.3. Evaluation of model parameters

This model employs kinetic and transport data related to hydrate formation available from previous research publications and other physical property data of gas components and water.

The gas phase consists of 10 typical natural gas components and their composition is measured using gas chromatography. The critical properties of the natural gas components were taken from Perry' Chemical Engineering Handbook [35]. The values of the above are given in Table 1.

At the given temperature, Langmuir constant values for gas components in hydrate cavities are calculated for structure II hydrates using Eq. (4), as it is this type of structure which would form in the presence of natural gas. The Kihara parameters for natural gas components and cavity characteristics were obtained from Ref. [15] and tabulated in Tables 2 and 3, respectively.

Table 2
Kihara parameters of natural gas components forming hydrates

| Component | $\xi = \varepsilon/k$ (K) | $\sigma$ (Å) | $a$ (Å) |
|---|---|---|---|
| $CO_2$ | 168.77 | 2.9818 | 0.6805 |
| $N_2$ | 125.25 | 3.0124 | 0.3526 |
| $CH_4$ | 154.54 | 3.1650 | 0.3834 |
| $C_2H_6$ | 176.40 | 3.2641 | 0.5651 |
| $C_3H_8$ | 203.31 | 3.3093 | 0.6502 |
| $iC_4H_{10}$ | 225.16 | 3.0822 | 0.8706 |
| $nC_4H_{10}$ | 209.00 | 2.9125 | 0.9379 |

Table 3
Cavity characteristics of structure II hydrates

| Cavity properties | Small | Large |
|---|---|---|
| Average cavity radius (Å) | 3.91 | 4.73 |
| Coordination number | 20 | 28 |
| Cavities per water molecule ratio | 2/17 | 1/17 |

The binary interaction coefficients for the natural gas components given below in Table 4 were obtained from Knapp and Doring [29].

Table 5 shows values of fitted parameter for Eqs. (11) and (12) for structure II hydrates, where $\Delta\mu^0_W$ value was taken from Ref. [36], and the values of $\Delta v^0_W$, $\Delta h^0_W$, and $\Delta C^0_{pW}$ from Refs. [37]. The values reported for the above parameters by several hydrate researches tend to differ and cause variations in predictions. The values used in this model for the above parameters were selected to closely match the equilibrium predictions from Sloan's CSMHYD© hydrate program for pure water [15].

The solubility of natural gas components in water was found from Henry's equation. The constants for Eq. (15) were again obtained from Ref. [15] and are given in Table 6. The solubility of heavy components pentane and hexane was ignored since they did not form hydrates and were of very small compositions in the gas.

The molar volumes for the natural gas component dissolved in water were obtained from Perry's Chemical Engineering Handbook (1997) (Table 7).

The activity of water in the presence of *p*TSA was determined using the UNIFAC group contribution method. The UNIFAC groups and their respective group parameters are given in Table 8. $R_k$ and $Q_k$ values for the respective groups were obtained from Reid et al. [32] except for the values of $ACSO_2$, which were obtained from Kang et al. [33].

The UNIFAC group interaction parameters for the above groups are given in Table 9. The group interaction parameters $Ac_{ij}$ are experimentally fitted parameters, obtained from Reid et al. [32]. The interaction parameters for $ACSO_2$ had not been reported to date; therefore interaction parameters for $ACNO_2$ were used instead, assuming that the interactions would be similar.

The only adjustable parameter in the model is the micelle size or aggregation number (*m*), which was adjusted to obtain a reasonable fit between the model and the experiment results. Details of which are discussed in the next section.

The hydrate equilibrium prediction models for pure water and *p*TSA–water systems were developed using Mathcad 2001i. Initially, the model for pressure predictions at given temperatures of pure water–natural gas–hydrates systems was developed using the equations in Section 2.1, and compared with the results of the CSMHYD© hydrate prediction program [15]. Subsequently equations in Section 2.2 were used together with equations in Section 2.1 to develop the model for equilibrium predictions of *p*TSA–water–natural gas–hydrates systems.

Table 4
Binary interaction coefficients of natural gas components

| | CO2 | N2 | C1 | C2 | C3 | IC4 | NC4 | IC5 | NC5 | C6 |
|---|---|---|---|---|---|---|---|---|---|---|
| CO2 | 0 | 0 | 0 | 0 | 0 | 0 | 0 | 0 | 0 | 0 |
| N2 | 0 | 0 | 0 | 0 | 0 | 0 | 0 | 0 | 0 | 0 |
| C1 | 0.0311 | 0.107 | 0.0 | 0 | 0 | 0 | 0 | 0 | 0 | 0 |
| C2 | 0.0515 | 0.1322 | 0.0026 | 0 | 0 | 0 | 0 | 0 | 0 | 0 |
| C3 | 0.0852 | 0.12413 | 0.0140 | 0.0011 | 0 | 0 | 0 | 0 | 0 | 0 |
| IC4 | 0.1 | 0.14 | 0.0256 | −0.0067 | −0.0078 | 0 | 0 | 0 | 0 | 0 |
| NC4 | 0.0711 | 0.1333 | 0.0133 | 0.0096 | 0.0033 | 0 | 0 | 0 | 0 | 0 |
| IC5 | 0.1 | 0.14 | −0.0056 | 0.0080 | 0.0111 | −0.004 | 0.017 | 0 | 0 | 0 |
| NC5 | 0.1 | 0.14 | 0.0236 | 0.0078 | 0.012 | 0.002 | 0.017 | 0 | 0 | 0 |
| C6 | 0.1496 | 0.1450 | 0.0422 | 0.014 | 0.0267 | 0.0240 | 0.0174 | 0 | 0 | 0 |

### 2.4. Experimental

The experiments were carried out in a constant volume PVT cell by varying the pressure–temperature conditions of a *p*TSA–water–natural gas system to form and dissociate hydrates. Hydrate phase equilibrium conditions were measured for the above system at three different concentrations of *p*TSA in water. The aim of these experiments was to thermodynamically quantify the influence of *p*TSA in a natural gas–water system.

#### 2.4.1. The PVT equipment

The pressure–volume–temperature equipment used in this experiment was designed and built by Sanchez Technologies France Ltd. (Fig. 1). The cell is rated at 1500 bars from temperatures of −20 to 200 °C and has a variable cell volume of 700 $cm^3$. The cell is constructed in two parts: the cylindrical stainless steel on the top and a much smaller (10 $cm^3$) sapphire cell with a window connected to an endoscope and then to a camera. The sensors used to acquire data are connected to a multi-channel analyser PC card (MCAPC card), which uses a sigma-delta 21 bit analog converter and is connected to the PC via a serial communication port RS422. The MCAPC card can be controlled via a software program called Falcon®, which is a macro-based language similar to PASCAL and the program is compiled in a code interpreted by Falcon. The software can be programmed to activate controls and to record data and display real-time graphs, which are vital in PVT experiments. The equipment measures pressures at accuracy levels of 0.1% of full scale using a HBM-type P3MB pressure sensor. The cell volume can be adjusted to accuracies of ±1 μl, where fibre optic sensors measure cell volumes and piston motor velocities.

Table 5
Equilibrium parameters for hydrate predictions

| Parameter | Value (J/mol) |
|---|---|
| $\Delta\mu_W^0$ | 883 |
| $\Delta v_w^0$ | |
| $T > T_0$ | 5.0 |
| $T < T_0$ | 3.4 |
| $\Delta h_W^0$ | |
| $T > T_0$ | −4781 |
| $T < T_0$ | 1230 |
| $\Delta C_{pW}^0$ | |
| $T > T_0$ | −36.86 |
| $T < T_0$ | 1.029 |
| $q$ | |
| $T > T_0$ | 0.1890 |
| $T < T_0$ | 0.0038 |

Table 6
Henry's constant parameters

| | H1 | H2 | H3 | H4 |
|---|---|---|---|---|
| CO2 | −317.658 | 17371.2 | 43.0607 | −0.002191 |
| N2 | −327.85 | 16757.6 | 42.84 | 0.016765 |
| C1 | −365.183 | 18106.7 | 49.7554 | −0.000285 |
| C2 | −533.392 | 26565.0 | 74.624 | −0.004573 |
| C3 | −628.866 | 31638.4 | 88.0808 | 0.0 |
| IC4 | 190.982 | −4913 | −34.5102 | 0 |
| NC4 | −639.209 | 32785.7 | 89.1483 | 0 |

Table 7
Molar volume of natural gas components

| Component | CO2 | N2 | C1 | C2 | C3 | IC4 | NC4 |
|---|---|---|---|---|---|---|---|
| Molar volume (l/mol) | 0.095 | 0.089 | 0.099 | 0.146 | 0.200 | 0.241 | 0.255 |

Table 8
UNIFAC groups and group parameters for *p*TSA and water system

| UNIFAC group | Main group no. | Secondary group no. | No. of groups | $R_k$ | $Q_k$ |
|---|---|---|---|---|---|
| ACH | 3 | 10 | 4 | 0.5313 | 0.400 |
| $ACCH_3$ | 4 | 12 | 1 | 1.2663 | 0.968 |
| OH | 5 | 15 | 1 | 1.0000 | 1.200 |
| $ACSO_3$ | 27 | 58 | 1 | 1.7034 | 1.160 |
| $H_2O$ | 7 | 17 | 1 | 0.9200 | 1.400 |

Table 9
UNIFAC group interaction parameters for *p*TSA and water

| | ACH | $ACCH_3$ | OH | $ACSO_3$ | $H_2O$ |
|---|---|---|---|---|---|
| ACH | 0 | 167 | 636.1 | 194.9 | 903.8 |
| $ACCH_3$ | −146.8 | 0 | 803.2 | 4448 | 5695 |
| OH | 89.6 | 25.82 | 0 | 157.1 | 353.5 |
| $ACSO_3$ | 1824 | −127.8 | 561.6 | 0 | 360.7 |
| $H_2O$ | 362.3 | 377.6 | −229.1 | 399.5 | 0 |

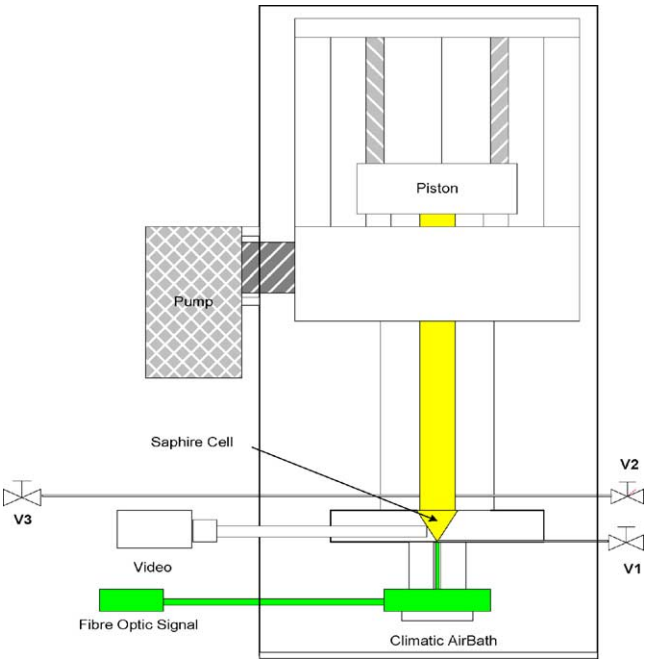


Fig. 1. Block diagram of PVT 1500/700 used for hydrate formation/ dissociation tests.

The temperature acquiring system measures at ±0.05% in its 253–473 K span using RTD sensors of PT100 type. More details of the PVT equipment can be found from the manufactures web site at http://www.stfrance.com.

### 2.4.2. Material

*2.4.2.1. pTSA/water solutions.* *para*-Toluene sulfonic acid monohydrate (98–100% purity) obtained form Sigma-Aldrich Chemicals in Perth, WA, is used with distilled water to prepare the solutions. A known amount of *p*TSA is weighted using an electronic weighing scale (accuracy: 0.05 g) and dissolved in a known quantity of distilled water. The concentrations tested were 1 g/l (1000 ppm), 3 g/l (3000 ppm) and 5 g/l (5000 ppm).

*2.4.2.2. Natural gas.* The natural gas used in the experiments was household gas or city gas supplied by Alinta Gas Ltd., Perth, Australia. The gas was first compressed into a *G* size cylinder and was tested for composition in the gas chromatography workstation. The mole fraction of the gas is given in Table 1.

### 2.4.3. Experimental procedure

The PVT apparatus was calibrated with natural gas for pressure–temperature measurements. The PVT cell was cleaned with water between same concentration experiments and was cleaned with acetone when different concentrations were used. The piston was lowered to zero volume of the cell and the pressure of the cell was calibrated to zero gauge pressure. The water–*p*TSA solution was loaded by drawing it into the cell by moving the piston up and increasing the cell volume. The cell volume was maintained constant at 200 and 100 $cm^3$ of the solution sample was loaded for all 'temperature cycling' tests. The solution was loaded from a measuring cylinder so that the sample could be measured within an accuracy of 1 $cm^3$. The gas was injected through a regulator from a *G* size cylinder into the cell through the connection (V-3) in the top of the cell. The gas pressure was selected according to pre-planned experimental intervals. The gas and liquid were allowed at room temperatures for half an hour for pre-experiment stabilisation. Then the temperature of the climatic air bath was decreased at an average cooling rate of 0.05 °C/min to the low-temperature limit. The lower temperature limit was selected to be within the hydrate formation zone allowing at least 10 °C of sub-cooling. The data recording in the computer was commenced as soon as the cooling was initiated. The variation of cell pressure, cell temperature and climatic air bath temperature were recorded and plotted in 10 s time intervals, along with the main plot of cell pressure against cell temperature, using the Falcon® software.

### 2.4.4. Experimental results

The time elapsed to form hydrates (induction time) varied depending on the test pressure and sample concentration. High-pressure tests and tests of 5 g/l *p*TSA showed relatively smaller induction times as compared to low-pressure tests and tests of 1 g/l *p*TSA. The formation of hydrates was recognised with a sudden and continuing fall in pressure in the pressure–temperature plot (see Fig. 4). After the initial steep drop in pressure, the pressure in the cell eased, indicating the near completion of hydrate formation in the cell or complete hydrate formation within the water–gas surface at least. The climatic air bath temperature set point was reversed to the higher temperature limit after allowing adequate time for hydrate formation. The high-temperature set point was selected to be around 10 °C higher than the possible equilibrium temperature. The cell was heated at an average rate of 0.03 °C/min to dissociate the hydrates formed. The cell temperature cycling pattern with time is shown in Fig. 2 for Experiment 1.1. The corresponding pressure variation with time is shown in Fig. 3. These curves were used in conjunction with the corresponding pressure–temperature curve (Fig. 4) to verify the hydrate equilibrium points. The cooling and heating periods along with the stabilisation period for a typical test is indicted in Fig. 2. The stabilisation period was maintained at lower temperature to ensure sufficient hydrate formation.

The pressure–temperature curve is also know as the 'temperature cycling curve' and is used to determine the hydrate equilibrium point. This point is located where a change in gradient is noted in the hydrate dissociation part of the pressure–temperature curve. At this point hydrates are completely dissolved and the gas starts to expand. The hydrate equilibrium point for Experiment 1.1 is shown in Fig. 4 (the corresponding point is also shown in pressure–time

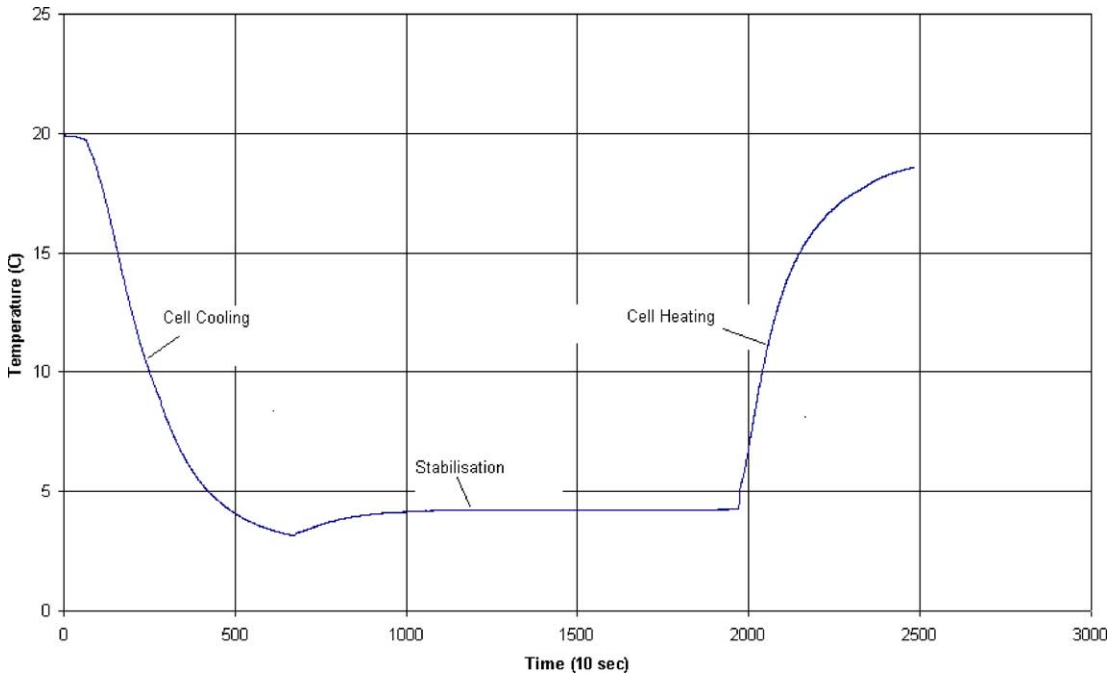


Fig. 2. Temperature vs. time curve for 1000 ppm TSA (Exp. no.: 1.1).

curve in Fig. 3). The point where hydrate formation starts is not a fixed point and is not considered as an equilibrium point due to the metastability exhibited by hydrates [15]. The equilibrium pressure–temperature point for smooth curves was estimated by considering the gradients of the two slopes of the curve. The equilibrium points from the temperature cycling experiments were then used to construct the equilibrium pressure–temperature dissociation curve for a particular natural gas–*p*TSA/water–hydrate system. The equilibrium points obtained from the 'temperature cycling' tests for the three different *p*TSA concentrations are tabulated along with the model predictions in Table 11.

### 2.5. Model evaluation

The pure water model predictions were compared with the results from the CSMHYD© hydrate prediction program [15] prior to the development of the *p*TSA–water model.

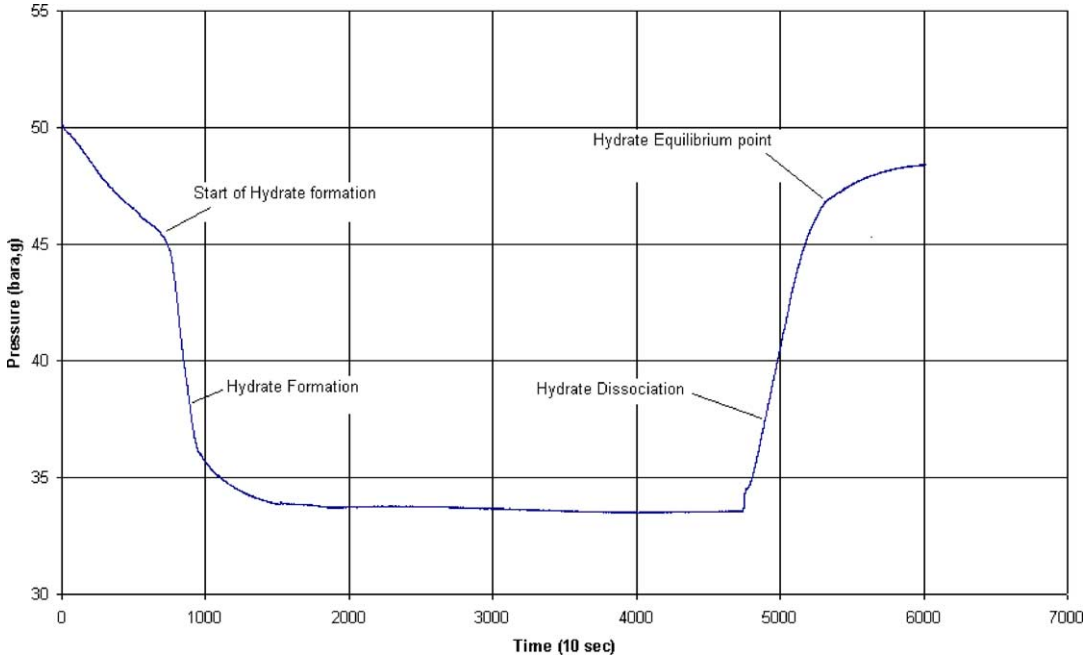


Fig. 3. Pressure vs. time curve for 1000 ppm TSA for (Exp. no.: 1.1).

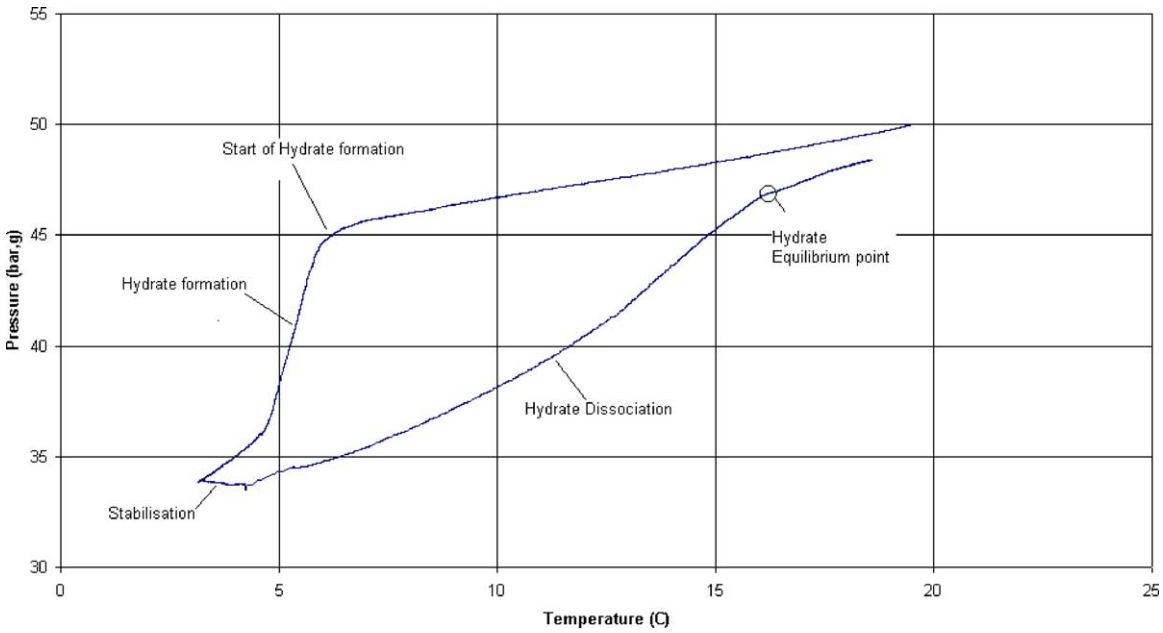


Fig. 4. Temperature cycling curve for determining equilibrium conditions (Exp. no.: 1.1).

The results showed very good compatibility between the two pure water models, with an average absolute deviations (AAD) percentage of around 1.11% (see Table 10). This strengthens the extension of the pure water model for predictions involving *p*TSA–water systems.

The model predictions for the three concentrations were obtained from adjusting the micelle size (*m*) to obtain a reasonable fit between the model and the experiment results. The model predictions and experimental results for the *p*TSA–water systems are tabulated along with the AAD values in Table 11, and the data are plotted in Fig. 5.

The hydrate prediction model for the *p*TSA–water–natural gas system shows appreciable agreement (overall AAD = 4.94%) with the experiment values obtained from the isochoric hydrates dissociation experiments.

The water activity coefficient calculated by the UNIFAC group contribution method for the organic solute *p*TSA–water system, showed minimal impact on the pure water hydrate equilibrium predictions at low solute concentrations, when incorporated into the pure water–gas hydrate prediction model in isolation. However, at a higher solute concentration (5000 ppm) the increase in water activity coefficient shifted the pure water–gas three-phase curve slightly to the left thus showing an inhibitive effect. This effect was negated when the aggregation behaviour of the micelles was incorporated into the final *p*TSA–water–gas–hydrate three-phase prediction model.

Table 10
Pure water systems: CSMHYD© and model predictions

| Temperature (°C) | *P* (CSMHYD©) (bara) | *P* (model) (bara) | Absolute error (%) |
|---|---|---|---|
| −3.15 | 6.69 | 6.57 | 1.83 |
| 1.85 | 9.60 | 9.20 | 4.22 |
| 6.85 | 17.39 | 16.64 | 4.30 |
| 11.85 | 31.75 | 30.60 | 3.63 |
| 16.85 | 61.72 | 60.34 | 2.23 |
| 21.85 | 149.76 | 150.50 | 0.50 |
| 26.85 | 349.57 | 358.60 | 2.58 |
| AAD (%) | | | 1.11 |

Table 11
*p*TSA–water systems: experimental and calculated values along with the AAD percentages

| Exp. no. | *T* (°C) | *P* (experiment) (bara) | *P* (model) (bara) | Absolute error (%) |
|---|---|---|---|---|
| 1000 ppm *p*TSA–water system | | | | |
| 1.6 | 13.31 | 28.82 | 31.91 | 10.72 |
| 1.2 | 15.89 | 38.90 | 44.77 | 15.09 |
| 1.1 | 16.23 | 47.90 | 46.90 | 2.09 |
| 1.3 | 17.52 | 57.52 | 56.33 | 2.07 |
| 1.4 | 18.45 | 67.83 | 64.77 | 4.51 |
| 1.5 | 18.72 | 74.88 | 67.55 | 9.79 |
| AAD (%) | | | | 4.49 |
| 3000 ppm *p*TSA–water system | | | | |
| 3.4 | 12.77 | 20.53 | 22.95 | 6.60 |
| 3.3 | 14.42 | 28.35 | 28.15 | 4.09 |
| 3.6 | 17.87 | 44.20 | 44.02 | 2.61 |
| 3.2 | 18.82 | 49.59 | 50.16 | 0.85 |
| 3.1 | 19.94 | 63.34 | 58.92 | 8.42 |
| 3.5 | 20.70 | 80.60 | 66.07 | 19.03 |
| AAD (%) | | | | 4.53 |
| 5000 ppm *p*TSA–water system | | | | |
| 5.7 | 11.87 | 14.11 | 14.78 | 4.75 |
| 5.8 | 15.05 | 24.50 | 21.81 | 11.00 |
| 5.6 | 15.79 | 18.96 | 23.90 | 26.05 |
| 5.5 | 16.69 | 25.78 | 26.73 | 3.69 |
| 5.4 | 18.48 | 36.75 | 33.54 | 8.73 |
| 5.2 | 20.83 | 53.25 | 45.73 | 14.12 |
| AAD (%) | | | | 5.80 |

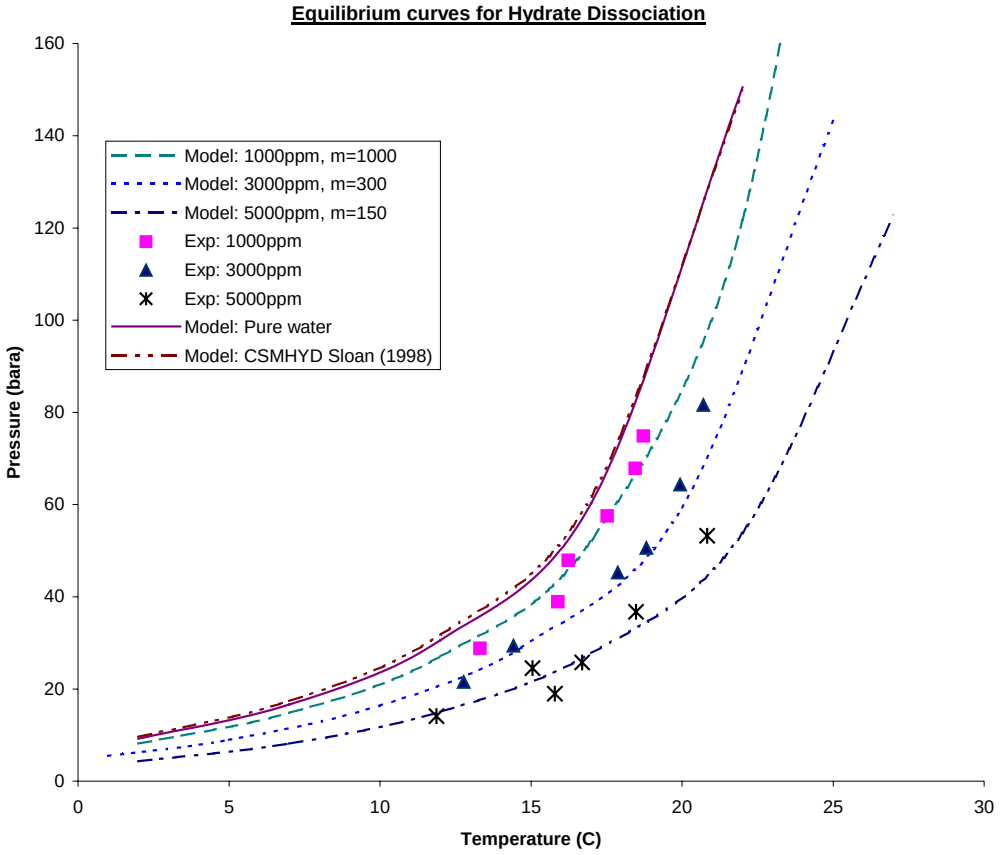


Fig. 5. Pure water and *p*TSA–water hydrate equilibrium curves.

The relationship between the adjustable parameter micelle size (or hydrotrope aggregation number), '*m*', and the concentration of monomeric hydrotrope, *p*TSA, was examined to formulate a relationship between the two. When plotted against each other, the micelle size showed a power law association with the monomeric concentration of *p*TSA (in ppm), as seen in Fig. 6. The following power law trend line equation with a '$R^2$' value of 0.9971 was obtained for the above system, indicating a high correlation between the hydrotrope aggregation number and *p*TSA monomeric concentration:

$$m = 3 \times 10^6 \,\text{ppm}^{-1.1656} \tag{24}$$

The above equation indicates an inverse relationship between the micelle size and the monomeric concentration of hydrotropes in the system. At low concentration the surface-active molecules are predominantly confined to the water–gas interface; therefore, the aggregation number or

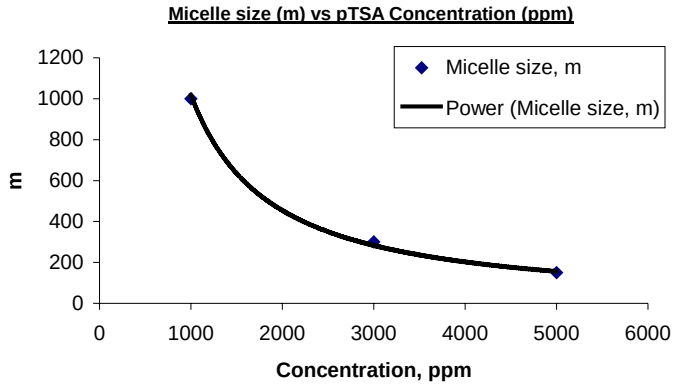


Fig. 6. The relationship between hydrotrope micelle size and *p*TSA concentration.

micelle size of the hydrotrope micelles would be high. On the other hand, with increasing hydrotrope concentration the micelles are formed throughout the solution and therefore the aggregation number or micelle size would decrease. Hence, an inverse relationship between monomeric hydrotrope concentration and micelle size is plausible. This relationship could only occur at very low concentrations of the hydrotrope–water system, and in our case it was assumed to be valid up to 5000 ppm *p*TSA in water. This phenomenon of surface-active agents could be due to the hydrotrope tendency to form loose aggregates rather than spherical micelles [38].

The above relationship in Eq. (24) would also hold at 0 ppm concentration of *p*TSA by reducing the model to the pure water model described in Section 2.1. This could be seen by substituting $x_0 \rightarrow 0$ and $m \rightarrow \infty$ in the chemical potential equation (23) where it reduces to the pure water chemical potential equation (16). This was verified by substituting $x_0 = 1$ and $m = 3 \times 10^6$ in the MathCad 2001i Model, where the hydrate formation predictions reduced to the pure water system.

## 3. Conclusion

The classical van der Waals–Platteeuw hydrate prediction model for pure water–gas system was extended to incorporate the activity of hydrotrope, *p*TSA, in water and the micelle aggregation behaviour, to predict the equilibrium hydrate formation condition of *p*TSA–water–natural gas–hydrate system. The aggregation behaviour of low concentration surface-active agent, such as hydrotrope in water, was incorporated within the thermodynamic hydrate prediction modelling systems for the first time. This model predicts the equilibrium pressure at a given temperature of the *p*TSA–water–natural gas–hydrate system for a given concentration of *p*TSA in water, between 0 and 5 g/l. The model predictions compare favourably with the experiment results for the three *p*TSA–water concentrations (AAD $\approx$ 5.0%). The adjustable parameter, the micelle size, could be calculated using the relationship given in Eq. (24) for a given *p*TSA concentration, and used directly in the calculations thus making it a priori prediction model. This a priori prediction model is used to develop a kinetic model for the hydrotrope *p*TSA–water–natural gas–hydrate system in a hydrate production spray reactor, details of which would be discussed in another publication [39].

*List of symbols*

| | |
|---|---|
| $a$ | guest core radius, equation of state parameter, activity |
| $C$ | Langmuir constant |
| $\Delta C_{p\mathrm{W}}$ | heat capacity difference of water at reference temperature |
| $f$ | fugacity |
| $h$ | enthalpy |
| $H$ | Henry's law constant |
| $k$ | Boltzmann's constant (J/K) |
| $m$ | micelle aggregation size |
| $N$ | constant ($N = 4$, 5, 10 or 11) |
| $p$ | number of gas components that occupy a particular cavity |
| $P$ | pressure |
| $P_\mathrm{c}$ | critical pressure |
| $q$ | constant for heat capacity equation |
| $Q$ | group parameter in UNIFAC calculations |
| $r$ | integration variable |
| $R$ | hydrate shell radius (Å), universal gas constant, group parameter in UNIFAC calculations |
| $T$ | temperature (K) |
| $T_\mathrm{c}$ | critical temperature |
| $v$ | molar volume ($\mathrm{cm}^3$/mol) |
| $V$ | number of groups in UNIFAC calculations |
| $x$ | liquid phase mole fraction |
| $x_0$ | monomeric *p*TSA mole fraction in liquid |
| $y$ | gas phase mole fraction |
| $z$ | coordination number, *z*-factor |

*Greek letters*

| | |
|---|---|
| $\gamma$ | activity coefficient |
| $\Gamma_k$ | group residual activity coefficient in UNIFAC calculations |
| $\delta$ | binary interaction coefficient |
| $\Delta$ | properties difference between liquid water and empty hydrate lattice |
| $\varepsilon$ | characteristic energy |
| $\theta$ | fractional occupancy of guests in the hydrate cavities, area fraction in UNIFAC calculation |
| $\mu$ | chemical potential (J/mol) |
| $\nu$ | number of cavities per water molecule in the hydrate lattice |
| $\varphi$ | fugacity coefficient, segment fraction in UNIFAC calculations |
| $\chi_i$ | mole fraction of group component in UNIFAC calculations |
| $\omega$ | cell potential function, acentric factor |

*Superscripts and subscripts*

| | |
|---|---|
| C | combinational term of the activity coefficient |
| H | hydrate |
| $i$ | arbitrary component |
| $j$ | arbitrary component |
| $k$ | group component in UNIFAC calculation |
| L | liquid |
| $m$ | total number of components in the gas mixture |
| $n$ | cavity type ($n = 1$ or 2) |
| R | residual term of the activity coefficient |
| W | water |
| 0 | property at reference condition |
| β | standard empty hydrate lattice |

## Acknowledgements

The authors wish to thank Woodside Energy Ltd., the project sponsor, for their continuing support to the Gas Hydrate Project at Curtin University of Technology, Western Australia, and their cooperation in publishing this paper.

## References

[1] J.H. van der Waals, J.C. Platteeuw, Advanced Chemistry and Physics, vol. 2, 1959.
[2] P. Englezos, P.R. Bishnoi, Am. Inst. Chem. Eng. 34 (1988) 1718–1721.
[3] F.E. Anderson, J.M. Prausnitz, Am. Inst. Chem. Eng. 32 (1986) 1321–1333.
[4] P. Englezos, Z. Huang, P.R. Bishnoi, J. Can. Petrol. Technol. 30 (1991) 148–155.
[5] P. Skovborg, P. Rasmussen, Chem. Eng. Sci. 49 (1994) 1131–1143.
[6] P. Englezos, N. Kalogerakis, P.D. Dholabhai, P.R. Bishnoi, Chem. Eng. Sci. 42 (1987) 2659–2666.
[7] P. Englezos, R. Kobayashi, P.D. Dholabhai, P.R. Bishnoi, Chem. Eng. Sci. 42 (1987) 2647–2658.
[8] J.P. Lederhos, J.P. Long, A. Sum, R.L. Christiansen, E.D. Sloan, Chem. Eng. Sci. 51 (1996) 1221–1229.
[9] Y.F. Makogon, S.A. Holditch, T.Y. Makogon, Ann. NY Acad. Sci. 715 (1994) 777–796.
[10] D. Kashchiev, A. Firoozabadi, J. Cryst. Growth 241 (2002) 220–230.
[11] D. Kashchiev, A. Firoozabadi, J. Cryst. Growth 243 (2002) 476–489.
[12] D. Kashchiev, A. Firoozabadi, J. Cryst. Growth 250 (2003) 499–515.
[13] J.S. Gudmundsson, V. Anderson, O.I. Levik, M. Parlaktuna, SPE Paper 50598, 1998.
[14] A. Fitzgerald, M. Taylor, SPE Paper 71805, 2001.
[15] E.D. Sloan, Clathrate Hydrates of Natural Gases, 2nd ed., Marcel Dekker, New York, 1998.
[16] M.D. Jager, R.M. De Deugd, C.J. Peters, J. de Swaan Arons, E.D. Sloan, Fluid Phase Equilibr. 165 (1999) 209–223.
[17] A.A. Khokhar, J. Gudmundsen, E.D. Sloan, Fluid Phase Equilibr. 150–151 (1998) 383–392.
[18] N. Kalogerakis, A.K.M. Jamaluddin, P.D. Dholabhai, P.R. Bishnoi, Soc. Petrol. Eng. SPE 25188 (1993) 375–383.
[19] N. Gnanendran, R. Amin, J. Petrol. Sci. Eng. 40 (2003) 37–46.
[20] Y. Zhong, R.E. Rogers, Chem. Eng. Sci. 55 (2000) 4175–4187.
[21] W.R. Parrish, J.M. Prausnitz, Ind. Eng. Chem. Res. Process. Des. Dev. 11 (1972) 26–34.
[22] D. Balasubramanian, V. Srinivas, V.G. Gaikar, M.M. Sharma, J. Phys. Chem. 93 (1989) 3870–3896.
[23] U. Karaaslan, E. Uluneye, M. Parlaktuna, J. Petrol. Sci. Eng. 35 (2002) 49–57.
[24] U. Karaaslan, M. Parlaktuna, Energy Fuels 15 (2001) 241–246.
[25] G.D. Holder, G. Gorbin, K.D. Papadopoulos, Ind. Eng. Chem. Fund. 19 (1980) 282.
[26] H.J. Ng, D.B. Robinson, Ind. Eng. Chem. Fund. 15 (1976) 293.
[27] V. McKoy, O. Sinanoglu, J. Chem. Phys. 38 (1963) 2946.
[28] G. Soave, Chem. Eng. Sci. 27 (1972) 1197–1203.
[29] H. Knapp, R. Doring, Vapour–liquid equilibria for mixtures of low boiling substances, DECHEMA, Frankfort, Germany (1982).
[30] I.R. Krichvsky, J.S. Kasaranovsky, J. Am. Chem. Soc. 57 (1935) 2168.
[31] K. Lekvam, P.R. Bishnoi, Fluid Phase Equilibr. 131 (1997) 297–309.
[32] R.C. Reid, J.M. Prausnitz, B.E. Poling, The Properties of Gases and Liquids, 4th ed., McGraw-Hill, New York, 1987.
[33] J.W. Kang, J. Abildskov, R. Gani, J. Cobas, Ind. Eng. Chem. Res. 41 (2002) 3260–3273.
[34] C. Tanford, The Hydrophobic Effect: Formation of Micelles and Biological Membranes, Wiley, New York, 1980.
[35] R.H. Perry, D.W. Green, J.O. Maloney, Perry's Chemical Engineers' Handbook, McGraw Hill, New York, 1997.
[36] J. Munck, S.S. Jorgensen, P. Rasmussen, Chem. Eng. Sci. 43 (1988) 2661–2672.
[37] G. Chen, T. Guo, Fluid Phase Equilibr. 122 (1996) 43–65.
[38] V. Srinivas, G.A. Rodley, K. Ravikumar, T. Robinson, M.M. Turbull, D. Balasubramanian, Langmuir 13 (1997) 3235–3239.
[39] N. Gnanendran, R. Amin, Chem. Eng. Sci., article in press.